5. Age of the Cenozoic Chaco foreland basin fill based on radiometric dating of tuffs

5.1 Introduction

The backarc of the Central Andes consists of ancient to recent retroarc foreland basins, whereas the actual foreland basin of the Central Andes is located along the eastern margin of the Andes, represented in southern Bolivia by the Chaco Basin. Ancient foreland basins are documented for the Altiplano, Eastern Cordillera, Interandean, and Subandean (e.g. Coudert et al., 1995; Dunn et al., 1995; Hérail et al., 1996; Kley, 1996; Schmitz and Kley, 1997; Horton, 1998; McQuarrie, 2002; DeCelles and Horton, 2003; McQuarrie et al., 2005).

Loading processes of orogens, such as the Central Andean orogen, account for deflection of the backarc lithosphere, which initiate the development of retroarc foreland basins (DeCelles and Gilles, 1996; Catuneanu et al., 1997; Horton et al., 2001, DeCelles and Horton, 2003, McQuarrie et al., 2005). Many scientists consider initial deformation processes within the backarc of the Central Andes as old as late Oligocene–early Miocene (e.g. Isacks, 1988; Sempere et al., 1990; Gubbles et al., 1993; Allmendinger et al., 1997; Jordan et al., 1997). Other scientists recognized an older deformation history in the Eastern Cordillera (e.g. Kennan et al., 1995; Lamb et al., 1997; Lamb and Hoke, 1997; Sempere et al., 1997; Horton, 1998; Horton et al., 2001; DeCelles and Horton, 2003; McQuarrie et al., 2005). Based on foreland basin deposits, several authors propose that a topographic high existed in the western part of the Central Andes as early as Cretaceous-Paleocene (Sempere et al., 1997; Horton et al., 2001).

Initial foreland basin development in the Central Andes is documented by Cretaceous to mid-Paleocene back-bulge deposits followed by mid-Paleocene to middle Eocene forebulge deposits throughout the Altiplano and Eastern Cordillera (Horton and DeCelles, 1997), as indicated by the Santa Lucia and Impora Formations (60-58 Ma; Sempere et al., 1997). At the same time proximal foredeep to wedge-top conditions are represented by the Purilactis Group in northeastern Chile (Horton et al., 2001).

Forebulge depositions was replaced by foredeep deposition in the eastern Altiplano and Eastern Cordillera during the late Eocene, which is documented by the Potoco Formation in the Altiplano and the Camargo Formation in the Eastern Cordillera (Horton and DeCelles, 2001; Horton et al., 2001). However, deviating source areas and lithologies of the Potoco and the Camargo Formations indicate two foredeep depozones with two fold-thrust systems, of which one is situated in the Western Cordillera and the other in the western Eastern Cordillera (McQuarrie et al., 2005). Growth strata and most proximal foreland basin conditions within the Tupiza basin suggest that the eastern front of the fold-thrust belt was situated in the central Eastern Cordillera (McQuarrie et al., 2005).

In the late Oligocene, forebulge to foredeep conditions (Dunn et al., 1995; Jordan et al., 1997) indicate an initial foreland basin evolution in the Subandean (McQuarrie et al., 2005). Time-equivalent continued foredeep deposition in the Altiplano and the Eastern Cordillera (Horton and DeCelles, 2001; Horton et al., 2001; DeCelles and Horton, 2003).

Early Miocene coarse-grained deposits in the Altiplano represent proximity to the fold-thrust belt (Baby et al., 1997; Sempere et al., 1990; Kennan et al., 1995). The east-vergent fold-thrust front reached time-equivalent the Interandean. Later on propagated the east-vergent fold-thrust front eastward. In the late Miocene entered the fold-thrust front the Subandean (McQuarrie et al., 2005), continued eastward propagation throughout the Subandean toward its actual position along the Subandean-Chaco border.

Because the foreland basin systems migrated eastward the depositional ages must have changed (Jordan et al., 1997; Echavarria et al., 2003; McQuarrie et al., 2005). I would like to address the following questions in this chapter: (1) What is the age of the five Cenozoic formations within the Subandean and the Chaco foreland basin? (2) Are these lithostratigraphically defined formations diachronous or remain constant? (3) What do the depositional ages of the Cenozoic formations tell us about foreland basin development?

5.1.1 Cenozoic formations of the Subandean-Chaco basin

During fieldwork in 2002 and 2003, I studied five lithologically defined formations within the Subandean and the Chaco: the Petaca, Yecua, Tariquia, Guandacay, and Emborozú Formations.

The Petaca Formation represents the base of the Cenozoic formations and contains soil horizons and braided light-red sandstone beds, interbedded by red to brown mudstone beds (Uba et al., in revision). The pedogenic facies indicate a forebulge depozone for the Petaca Formation, after the definition of DeCelles and Giles (1996). Marshall et al. (1993) postulate a depositional age of ~27 Ma for the Petaca-base, related to mammal bones along the Quebrada Saguayo, in the westernmost Chaco (Fig. 5.1). The depositional age of the Petaca-top is dated by Marshall et al. (1993) of Chasicoan-Montehermosan age (middle/late Miocene-early Pliocene), based on the occurrence of armadillo *Vassallia minuta* found along the Rio Yapacani (Fig. 5.1).

The overlying Yecua Formation documents a wetland environment with thick red to brown mudstone beds which are interbedded with thin-bedded sandstone beds, coarse-grained cross-bedded sandstone beds, shell hash coquinas, and thinly interbedded sandstone-mudstone-couplets (chapter 3). The lithologies suggest overbank, lacustrine and restricted marginal marine facies (chapter 3) deposited in a distal foredeep depozone. Biostratigraphic correlation of foraminifera suggests a depositional age of middle-late Miocene (14-7 Ma) for the marine Yecua facies (chapter 3), which is comparable with the specification of Marshall et al. (1993) that the deposition of the Yecua Formation took place between Colhuehiapian-Chasicoan (middle early to early late Miocene), documented by litoptern cf. *Theosodon* sp. along the Rio Moile.

The Tariquia, Guandacay, and Emborozú Formations represent a classical terrestrial foredeep to wedge-top sequence (Fig. 5.2) with increasing stream power from the Tariquia Formation toward the Emborozú Formation and consistently west-to-east transport direction (Uba et al., in revision). In addition, petrological studies indicate increasing influence of recycled orogen source for these formations (chapter 2). The Tariquia Formation consists of interbedded sandstone and mudstone with decreasing mudstone content from the base to the top, indicating a distal to proximal foredeep depozone. Fish fossils at the base of the Tariquia Formation (Marshall and Sempere, 1991) indicate a Chasicoan-Huaquerian age (middle-late Miocene, 12-5.3 Ma) along the Rio Moile (Fig. 5.1). However, our biostratigraphic study (chapter 3) suggests that the base of the Tariquia Formation may be approximately 7 Ma old.

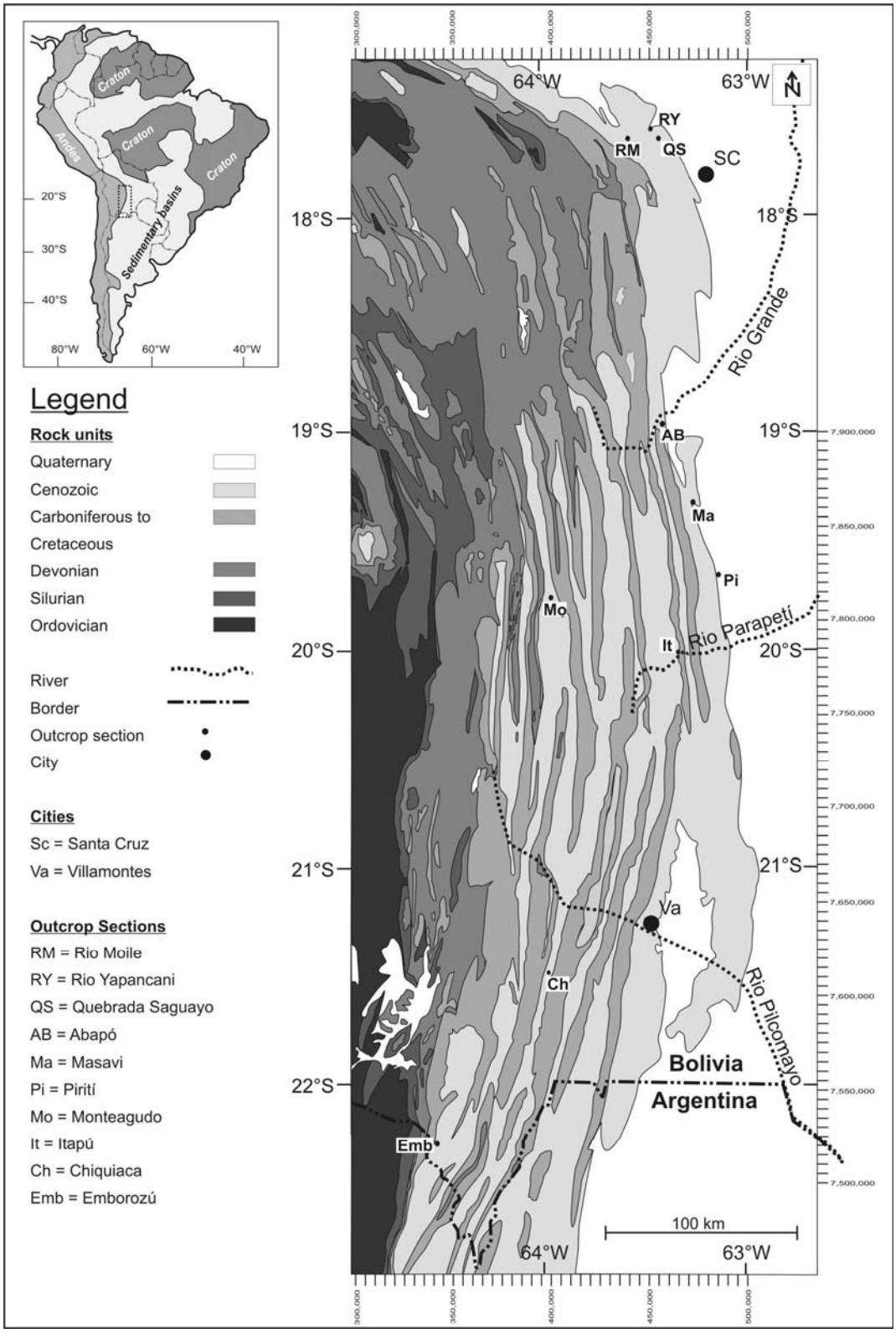

Fig. 5.1: (A): Overview of the major geological provinces of the South American continent. Dashed line shows the sketch of B. (B): Geological map (modified after Reutter et al., 1994) of the northern part of the Chaco Basin, showing sample locations and geographical locations that are mentioned in the text.

The deposits of the Guandacay Formation are composed of gravel-bearing sandstone interbedded with thin mudstone. The deposits indicate braided stream transport along a very proximal foredeep position. Marshall and Sempere (1991) described the skeleton of a

notoungulate along the base of the Guandacay Formation near Bermejo (Fig. 5.1), suggesting a Chasicoan-Huayquerian age (12-5.3 Ma). However, Moretti et al. (1996) documented that the angular discontinuity between the Tariquia Formation and the Guandacay Formation near Villamontes (Fig. 5.1) is of late Miocene age (6 Ma).

The Emborozú Formation consists of thick beds of conglomerates and thick beds of sandstone beds, indicating alluvial fan deposits within a wedge-top depozone. Moretti et al. (1996) postulated a depositional age of the Emborozú-base of Late Pliocene (3.3 Ma), based on radiometric age data of a tuff bed along the Guandacay-Emborozú contact near Abapó.

5.2 Sample description

Cornelius Uba and I sampled thirteen tuffaceous beds from dry stream banks or roadside outcrops along the synclines of the Subandean belts (Fig. 5.1). Tab. 5.1 shows the location names and coordinates of the samples, as well as their stratigraphic position.

Tab. 5.1: List of tuff samples, given with section name (see also Fig. 5.1), coordinates and formation names.

Sample number	Section	W-coordinate (UTM)	S-coordinate (UTM)	Formation
Abapó-1	Abapó	451438	7907906	Emborozú
CH-095	Piritί	484348	7822397	Pleistocene
CH-160	Masavi	469506	7857356	Tariquia
CH-318	Itapú	467678	7784758	Petaca
CH-01	Chiquiaca	399853	7622534	Tariquia
Emb-01	Emborozú	342355	7534539	Emborozú
Emb-02	Emborozú	342702	7534584	Emborozú
Emb-04	Emborozú	342942	7531975	Emborozú
Emb-05	Emborozú	342942	7531975	Emborozú
Emb-06	Emborozú	344401	7530956	Tariquia
Emb-07	Emborozú	345013	7529336	Tariquia
Emb-10	Emborozú	344038	7520166	Tariquia
Emb-11	Emborozú	344092	7518941	Tariquia

Sample Abapó-1 was taken from a tuff bed along the river cut of the Rio Grande several kilometers west of the village of Abapó (Fig. 5.1). The tuff bed is approximately 1.8 m thick and appears dark blue to grey, fine-grained with a high content of biotites (Fig. 5.2). The underlying bed is composed of well-rounded, imbricated conglomerate; the overlying bed consists of yellow to red sandstones. The depositional environment of the surrounding beds represent an alluvial fan of the Emborozú Formation.

Sample CH-095 was part of a tuff bed that crops out in a dry stream bank approximately 18 km north of Charagua (Fig. 5.1). The tuff bed is 2.0 m thick, is light grey, fine- to medium-grained, has a high biotite content, and shows a fining-upward trend (Fig. 5.2). The tuff bed shows a sharp base with erosional relief, hummocky cross-stratification, or scour and fill structures. The bed is interbedded with horizontal, sandy, unconsolidated material.

The tuff bed of sample CH-160 crops out in a dry stream bank near the village of Masavi (Fig. 5.1). It is fine-grained, of grey to yellow color, consists of high content of very fine-grained biotites, and is 10 cm thick. The tuff bed is comprised of multiple layers, including interbedded tuff and background sediments, which pinch and swell along the outcrop. The tuff is interbedded with medium-cross-bedded, red to yellow sandstones and subordinate maroon

mudstones, characterizing an anastomosing fluvial megafan of the Tariquia Formation, deposited in a foredeep zone.

Sample CH-318 was taken from a tuff bed that crops out for 7 cm within the section Itapú along the Rio Parapetí (Fig. 5.1). The tuff is fine-grained, contains a high content of very fine grained biotite, and has a grey to yellow color (Fig. 5.2). Under- and overlying red to brown sandstones are medium- to coarse-grained, very quartz-rich, and interbedded with brown mudstone beds that indicate a braided stream of the upper Petaca Formation approximately 15 m below the Yecua-Petaca contact.

Fig. 5.2: Photographs of the tuff beds within the Cenozoic sediments of the Subandean-Chaco Basin. Left: Tuff beds from the Petaca Formation, Itapú section; center: Emborozú Formation, Abapó section; right: Quaternary deposits, Piritί Formation.

CH-01 represents an outcrop from a river cut of the Rio Tarija in section Chiquiaca (Fig.5.1). Unfortunately, the tuff is exposed for several meters only. The outcrop represents medium cross-bedded, red to yellow sandstones and brown mudstones. We interpreted a fluvial deposition of the Tariquia Formation deposited in a foredeep zone.

The samples EMB-01 – EMB-11 derive from roadside outcrops along the Emborozú - Bermejo road, near the village of Emborozú. Sample EMB-01 and EMB-02 crop out at the western flank of the Emborozú syncline, whereas the samples EMB-04 – EMB-11 are from the eastern flank of the Emborozú syncline.

Sample EMB-01 is from a 70 cm thick, dark grey to black tuff that is interbedded in an overbank deposit within cobble-conglomerates. The approximately 4 m thick overbank deposit also contains red sandstones and brown mudstones. However, the conglomerates over- and underlying the overbank facies indicate alluvial fan deposits of the Emborozú Formation.

Sample EMB-02 was taken from a black to dark grey, 30 cm thick tuff bed, interbedded in thick cobble- and boulder-conglomerates. The depositional environment is identical to sample EMB-01, representing alluvial fan deposits of the Emborozú Formation.

Sample EMB-04 comes from a dark gray tuff bed, interbedded in dark red to grey muddy overbank sandstone. Thick conglomerates over- and underlay the overbank facies and indicate an alluvial fan environment of the Emborozú Formation.

Sample EMB-05 represents a very thin (less than 10 cm) tuff bed, has dark gray color, and deposited within thick conglomerates of the Emborozú Fm, indicating an alluvial fan environment.

Sample EMB-06 derives from black to dark grey tuff of 30 cm thickness. The underlying bed consists of a red to orange, medium-grained sandstone bed deposited in a braided stream,

whereas the overlying bed represent interbedded sandstone-mudstone beds of an overbank deposit. The lithology indicates that the tuff sample is part of the Tariquia.

Sample EMB-07 represents a 20 cm thick, grey tuff bed. The underlying bed contains red to yellow, medium-grained, cross-bedded sandstone with rip-up clasts, deposited in an anastomosing stream. The overlying beds represent interbedded sandstone-mudstone beds of an overbank deposit. The lithology indicates that the tuff bed was deposited within the Tariquia Formation.

Sample EMB-10 was taken from a blue-grey tuff bed that crop out for 20 cm and which is interbedded with red to orange medium-grained sandstones of the Tariquia Formation.

Sample EMB-11 represents a 10 cm thick grey tuff. The underlying bed contains red to orange medium-grained sandstone, whereas the overlying bed represent interbedded sandstones-mudstones of an overbank deposit. The lithologies indicate that the tuff was deposited within the Tariquia Formation.

5.3 Methods

We measured biotites from the tuffs using the Ar-Ar dating technique. This method is based on the decay of ^{40}K to ^{40}Ar and follows the same principles as the ^{40}K-^{40}Ar dating technique (Merrihue, 1965; Merrihue and Turner, 1966).

5.3.1 Sample preparation and experimental procedure

The samples were first checked for the presence of biotite in hand samples and in thin sections. After sample crushing, magnetic separation, heavy liquid separation, and handpicking in the mineral separation laboratory of the FU Berlin, we sent the prepared biotite samples for irradiation to a reactor in Canada. After irradiation and cooling, we measured the isotopic contents in the laboratory of Prof. Igor Villa, Universität Bern, Switzerland. $^{40}Ar/^{39}Ar$ analysis were carried out with a modified MAP® 215-50B rare gas mass spectrometer fitted with a Merchantek® quadroupled Nd-YAG laser, using the $^{40}Ar/^{39}Ar$ step heating method of dating. Heating for 10-30 minutes per step followed a schedule of 7-13 steps per sample.

5.3.2 Introduction of technique

In the $^{40}Ar/^{39}Ar$ modification of the K-Ar technique, a biotite-sample is irradiated with fast neutrons, thereby converting ^{39}K to ^{39}Ar through a (n,p) reaction (Dalrymple and Lanphere, 1974). Following irradiation, the sample is incrementally heated and the gas analyzed in the same manner as in the conventional K-Ar procedure. Some of the advantages of the $^{40}Ar/^{39}Ar$ method over the conventional K-Ar technique are:

1. A single analysis is conducted on one aliquot of sample, thereby reducing the sample size and eliminating sample inhomogeneity.
2. Analytical error incurred in determining absolute abundances is reduced by measuring only isotopic ratios. This also eliminates the need to know the exact weight of the sample.
3. The sample does not need to be completely fused, but rather can be incrementally heated. The $^{40}Ar/^{39}Ar$-ratio (age) can be measured for each fraction of argon released; this allows the generation of an age spectrum.

The age of the biotite sample can than be calculated by the $^{40}Ar^*/^{39}Ar_K$-ratio, where $^{40}Ar^*$ represents the radiogenic argon and $^{39}Ar_K$, the Ar-isotope produced from ^{39}K by irradiation. The $^{40}Ar^*/^{39}Ar_K$ is corrected by atmospheric ^{40}Ar and other isotopic interferences (Ca, K, and Cl) due to irradiation. The age of the sample is obtained by the following equation (Dalrymple and Lanphere, 1974):

$$t = 1/\lambda * \ln[(^{40}Ar^*/^{39}Ar_K)*J+1]$$

, where J = specific parameter of the biotite sample which affects the samples during irradiation. This parameters be defined by comparing the measured $^{40}Ar/^{39}Ar$-ratio with that of a standard of known age,

and λ = the total decay constant of ^{40}K ($5.543*10^{-10}$).

During analyses, Ar is liberated by several heating stages, called incremental or stepwise heating procedure (Merrihue, 1965). Step heating refers to the stepwise degassing of a sample with increasing temperatures up to a temperature were all Ar is heated. The tables (Appendix E) and figures (5.3 to 5.11) include individual step ages of each incremental heating step, total gas ages, which represent the age average of all measured argon peaks for all steps, age spectrum, and inverse isochron age.

Age spectrum plots show the age of each incrementally heated gas fraction versus the cumulative $^{39}Ar_K$ released, with steps increasing in temperature from left to right. Each apparent age is calculated assuming that the trapped argon (argon not produced by in situ decay of ^{40}K) has the modern day atmospheric $^{40}Ar/^{36}Ar$-value of 295.5. Additional K/Ca-ratios (determined from measured Ca-derived ^{37}Ar and K-derived ^{39}Ar) for each heating step are plotted versus cumulative % $^{39}Ar_K$ released. Incremental heating analysis may reveal complex argon systematics related to excess argon, alteration, contamination, ^{39}Ar recoil, or argon loss (Merrihue, 1965). Often low-temperature heating steps have low radiogenic yields and apparent ages with relatively high errors due mainly to loosely held, non-radiogenic argon residing on grain surfaces or along grain boundaries. An entirely or partially flat spectrum of plateau age, in which apparent ages are the same within analytical error, may indicate that the sample is homogeneous with respect to K and Ar and has had a simple thermal and geological history. A criterion for a plateau age is the identification of a series of adjacent steps (more than 2), which together comprise more than 50% of the total Ar release, each of which yields an age within the standard deviations (2σ) of the mean (Dalrymple and Lanphere, 1974; Lee et al., 1991).

Another method to display the $^{40}Ar^*/^{39}Ar_K$-ratio is the inverse isochron analysis, where the $^{39}Ar/^{40}Ar$ ratio is plotted against $^{36}Ar/^{40}Ar$-ratio. The isochron analysis can permit the detection of possible excess or loss of argon. If the sample was not affected by Ar excess or Ar loss, steps with the same age fall on a line with the $^{40}Ar/^{39}Ar$-ratio equal to atmospheric $^{40}Ar/^{39}Ar$ (295.5; York, 1969).

5.4 Results

Figures 5.3 – 5.11 show the age spectrum for each sample and plot the apparent K/Ca-ratio of each step against the cumulative $^{39}Ar_K$ released. Statistical errors are graphically displayed at the 2σ confidence level. Inverse isochron plots ($^{36}Ar/^{40}Ar$ vs. $^{39}Ar/^{40}Ar$) are also shown.

5.4.1 Ar-Ar data of a tuff sample from the Petaca Formation (CH-318)

The total gas age of sample CH-318 amounts to 23.5 ± 5.2 Ma. The age spectrum displays a staircase profile in which the apparent $^{40}Ar/^{39}Ar$ age descends continuously from the first step with a date of ~93 Ma to more constant dates for the mid- to high-temperatures in which the apparent ages range between 27.0 -18.5 Ma. Steps 3 to 7, which represent more than 90 % of the cumulative ^{39}Ar content, yield an integrated age of 22.7 ± 4.0 Ma (Fig. 5.3B) and an isochron age of 20.8 ± 1.5 Ma (Fig. 5.3C). Lo and Onstott (1995) describe age spectrum profile as very similar to those expected for argon loss. The K/Ca-ratios between step 3-7 are roughly constant (Fig. 5.3A). Steps 1, 2, and 8 are to low to implement further interpretation. However, no plateau appears, thereby the integrated and the isochron age can be discarded as to the interpretation of a depositional age.

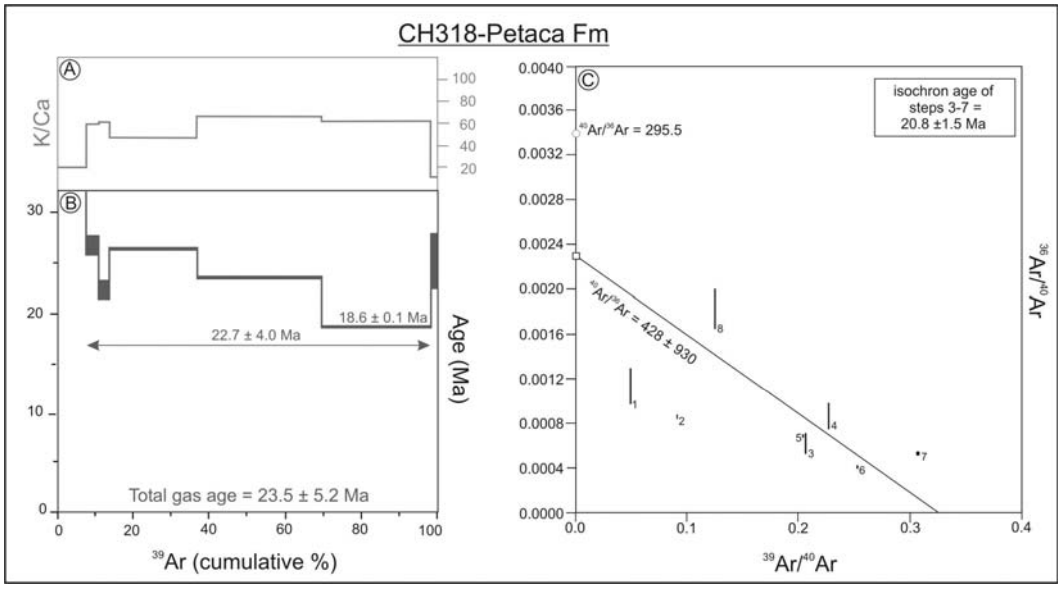

Fig. 5.3: Radiometric data of biotite sample CH-318. (A) Plot of the K/Ca-ratio versus cumulative ^{39}Ar; (B) $^{40}Ar/^{39}Ar$ incremental heating age spectra; (C) $^{40}Ar/^{39}Ar$ inverse isochron diagram. Circle shows the atmospheric $^{40}Ar/^{36}Ar$-ratio, grey dashed line is the intercept of all data points, and black solid line represents the intercept of the integrated age. See text for discussion. The result of each step is given in Appendix E. Analytical uncertainties are reported at the 2σ level.

We assume that the total gas age of 23.5 ± 5.2 Ma represents a likely depositional age. Most probably, the biotite has a maximum depositional age of 18.6 Ma (step 7 with an amount of 29 % ^{39}Ar).

5.4.2 Ar-Ar data of tuff samples from the Tariquia Formation

CH-160

Sample CH-160 represents a total gas age of 356 ± 22 Ma. The age spectrum profile shows an irregular distribution between 402 and 330 Ma. Steps 1 to 5 behaved during the measurement "dirty" and have to be excluded from age interpretation. The integrated age of steps 6-8 is 348 ± 8 Ma with an isochron age of 348 ± 6700 Ma. However, also the steps 6-8 also represent K/Ca-ratios too low for datable biotite-samples (Fig. 5.4A), suggesting that the measured sample does not present a meaningful age. Therefore, sample CH-160 will be excluded from the discussion below.

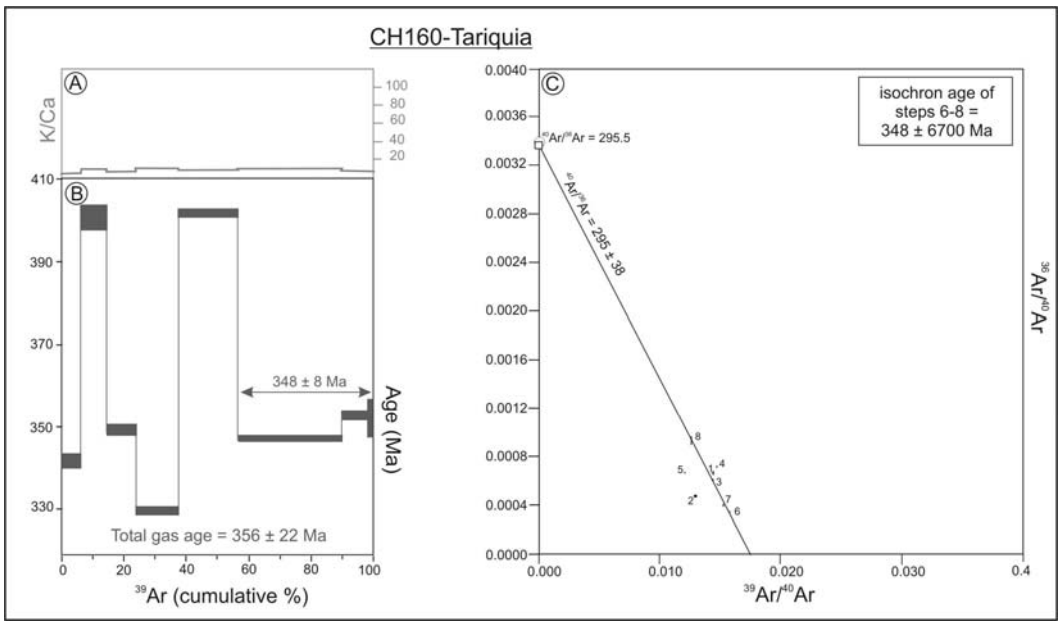

Fig. 5.4: Radiometric data of biotite sample CH-160. (A) Plot of the K/Ca-ratio versus cumulative ^{39}Ar; (B) $^{40}Ar/^{39}Ar$ incremental heating age spectra; (C) $^{40}Ar/^{39}Ar$ inverse isochron diagram. Circle shows the atmospheric $^{40}Ar/^{36}Ar$-ratio, grey dashed line is the intercept of all data points, and black solid line represents the intercept of the integrated age. See text for discussion. The result of each step is given in Appendix E. Analytical uncertainties are reported at the 2σ level.

CH-01

Sample CH-01 documents a total gas age of 9.41 ± 0.52 Ma. The age spectrum exhibits relatively old dates in the low-temperature steps and remains fairly flat during the later temperature steps (steps 4-8; Fig. 5.5B); however, no plateau age exist. Lo and Onstott (1995) suggested that the anomalously old dates in low-temperature steps may have resulted from the presence of exsolved phases. The K/Ca-plot shows medium ratios in the low-temperature steps (1-4), high ratios in the moderate-temperature steps (5 and 6), and moderate to low ratios in the high temperature steps (7-8; Fig. 5.5A). The intercept age of steps 5 and 6 (with >72 % ^{39}Ar) amounts to 9.30 ± 1.50 Ma and the isochron age of steps 5 and 6 accounts for 8.55 ± 0.19 Ma. However, these ages are insufficient because the two steps do not define a valid plateau. For further interpretation, we assume that the total gas age of 9.41 ± 0.52 Ma demonstrates best the depositional age of the sample CH-01.

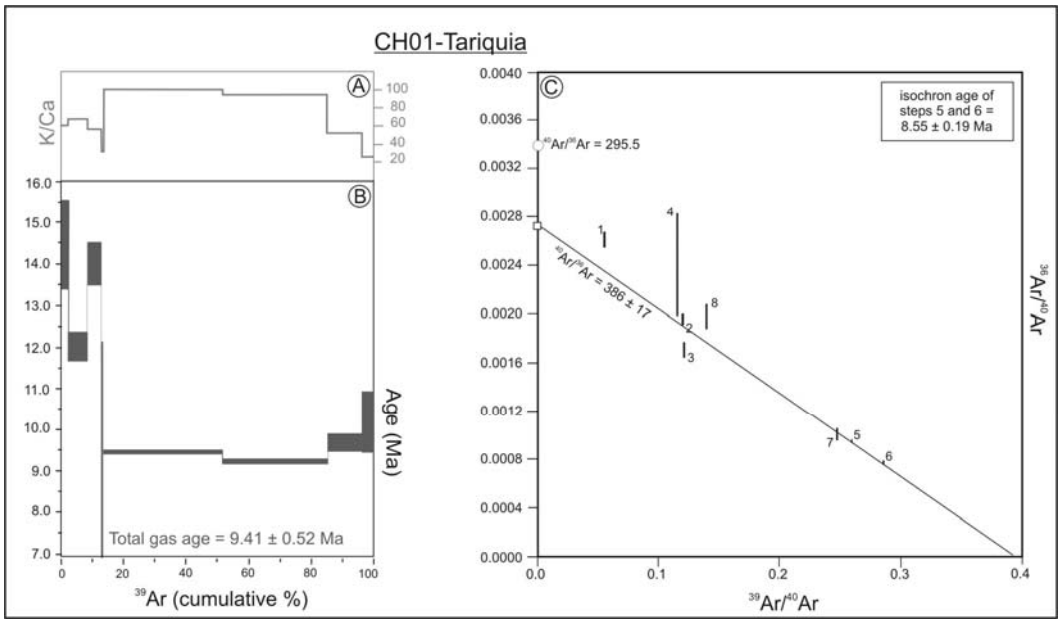

Fig. 5.5: Radiometric data of biotite sample CH-01. (A) Plot of the K/Ca-ratio versus cumulative ^{39}Ar; (B) ^{40}Ar/^{39}Ar incremental heating age spectra; (C) ^{40}Ar/^{39}Ar inverse isochron diagram. Circle shows the atmospheric ^{40}Ar/^{36}Ar-ratio, grey dashed line is the intercept of all data points, and black solid line represents the intercept of the integrated age. See text for discussion. The result of each step is given in Appendix E. Analytical uncertainties are reported at the 2σ level.

EMB-06

Samples EMB-06 (total gas age of 9.05 ± 0.73 Ma) shows an age spectrum in which apparent ages are low in the second step, rise to the fourth step, and end in a flat for the mid- and high-temperature (Fig. 5.6B). The origin of the disturbed ages in the initial steps (Lo and Onstott, 1989) may reflect the combined result of differential degassing of intercalated chlorite and partially reset biotite, as well as the internal recoil of ^{39}Ar, which occurred during irradiation. The flat region demonstrates a plateau age of 8.88 ± 0.07 Ma for steps 6-8. The intercept of the sample EMB-06 is equivalent to the atmospheric intercept and the isochron age is 8.92 ± 0.10 Ma (Fig. 5.6C). However, the K/Ca plot of sample EMB-06 is moderate to very low for the plateau steps. The total gas age of 9.05 ± 0.73 Ma therefore represents a likely depositional age of the sample EMB-06.

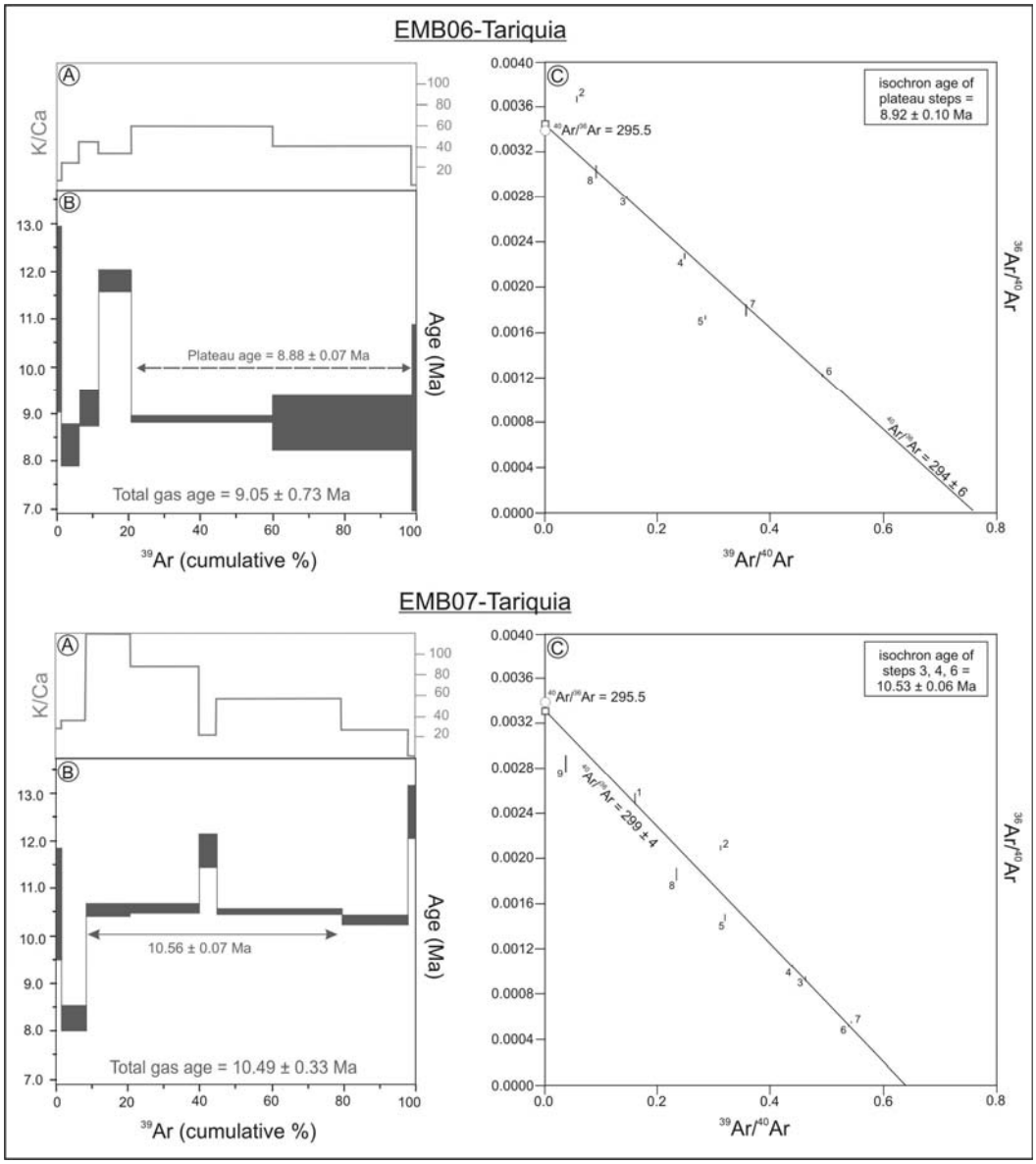

Fig. 5.6: Radiometric data of biotite samples EMB-06 and EMB-07. (A) Plot of the K/Ca-ratio versus cumulative ^{39}Ar; (B) $^{40}Ar/^{39}Ar$ incremental heating age spectra; (C) $^{40}Ar/^{39}Ar$ inverse isochron diagram. Circle shows the atmospheric $^{40}Ar/^{36}Ar$-ratio, grey dashed line is the intercept of all data points, and black solid line represents the intercept of the integrated age. See text for discussion. The result of each step is given in Appendix E. Analytical uncertainties are reported at the 2σ level.

EMB-07

EMB-07 (total gas age of 10.49 ± 0.33 Ma) shows an age spectrum in which apparent ages are low in the second step and rise to a flat for the mid- and high-temperature (Fig. 5.6B). The flat region of sample EMB-07 is disturbed by a hump at intermediate temperature (step 5) and displays an integrated age of 10.59 ± 0.07 Ma for steps 3, 4, 6, and 7. The hump-effect is typical for chloritized biotite with excess argon residing in chlorite (Lo and Onstott, 1989). The K/Ca-plot indicates decreasing ratios for the integrated steps, whereas the ratio is high for steps 3 and 4, moderate for step 6, and low for step 7 (Fig. 5.6A). Therefore we calculated the intercept of the isochron diagram for steps 3, 4, and 6 with 299 ± 4 equivalent to the atmospheric $^{40}Ar/^{36}Ar$-ratio and with an isochron age of 10.53 ± 0.06 Ma (Fig. 5.6C). We suggest that the total gas age of 10.49 ± 0.33 Ma represents the most likely depositional age of sample EMB-07.

EMB-10

The total gas age of sample EMB-10 yields 9.67 ± 0.58 Ma. The age spectrum shows a double upward-convex form, in which the initial steps are low and rise to a flat, before decreasing again two a second flat region in the mid-temperature range, and then rise again in the last steps (Fig. 5.7B). Lo and Onstott (1995) observed these behavior for biotites that are substantially altered to an assemblage of chlorite, sphene, and quartz. Steps 1-4 behave like a "dirty sample". However, steps 1-3 show high K/Ca-ratio, whereas the K/Ca-ratio of the other steps is low to very low (Fig. 5.7A). Therefore, we do not calculate an isochron (Fig. 5.7C) or integrated age and assume that the total gas age of 9.67 ± 0.58 Ma represents the most possible depositional age of sample EMB-10.

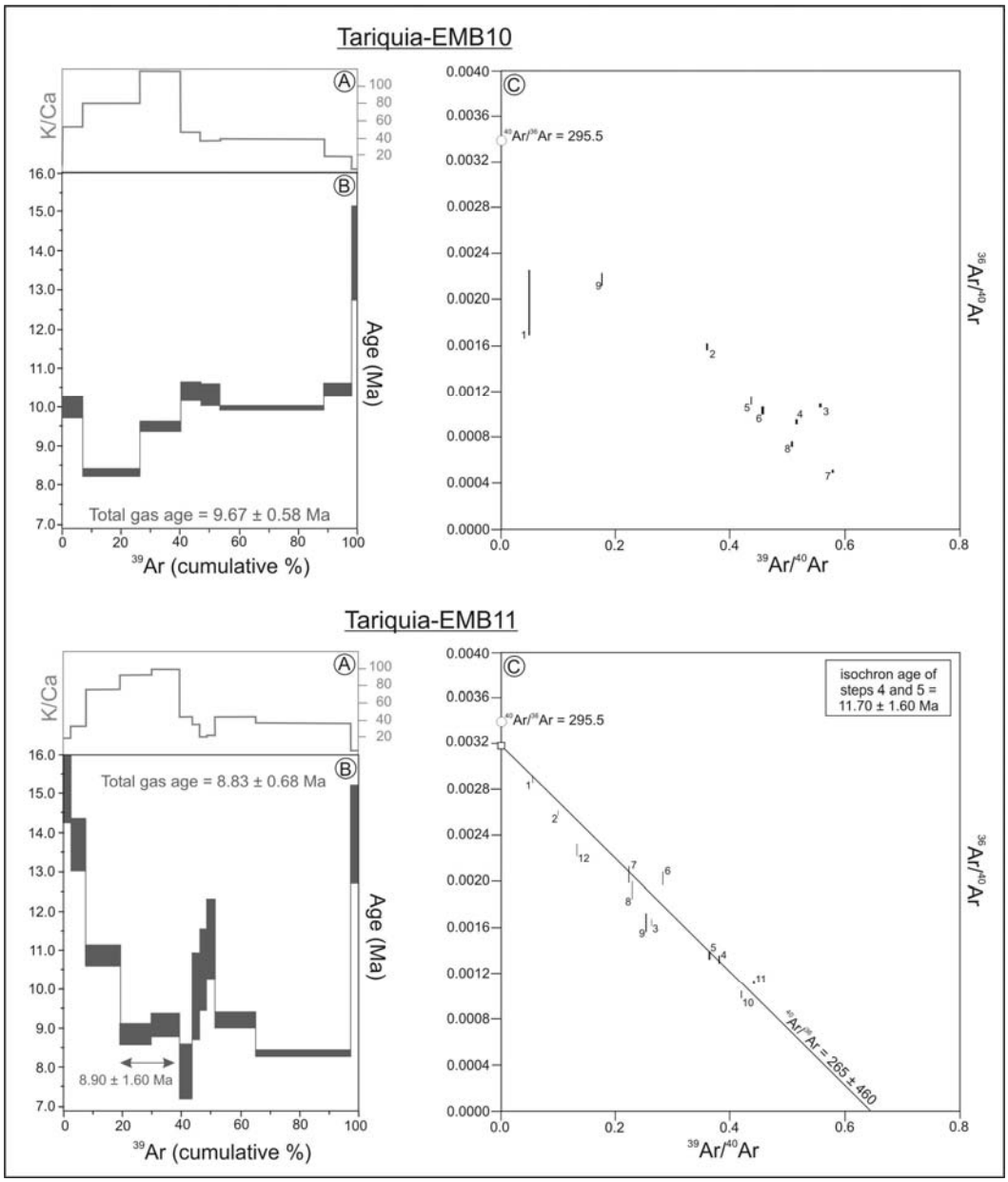

Fig. 5.7: Radiometric data of biotite samples EMB-10 and EMB-11. (A) Plot of the K/Ca-ratio versus cumulative ^{39}Ar; (B) $^{40}Ar/^{39}Ar$ incremental heating age spectra; (C) $^{40}Ar/^{39}Ar$ inverse isochron diagram. Circle shows the atmospheric $^{40}Ar/^{36}Ar$-ratio, grey dashed line is the intercept of all data points, and black solid line represents the intercept of the integrated age. See text for discussion. The result of each step is given in Appendix E. Analytical uncertainties are reported at the 2σ level.

EMB-11

Sample EMB-11 (total gas age of 8.83 ± 0.68 Ma) shows a saddle-shaped age spectra. The first steps yields very high apparent ages, mid-temperature steps define a flat region with a hump effect for steps 6-9, and the very high-temperatures results in apparent high ages again (Fig. 5.6B). The K/Ca-plot indicates high ratios for steps 3-5 and low to very low ratios for the other steps. The intercept of the steps 4 and 5 indicates an age of 8.90 ± 1.60 Ma and the isochron plot suggests an ages of 11.70 ± 1.60 Ma. However, two steps alone are not sufficient for a geological interpretation; we therefore assume a total gas age of 8.83 ± 0.68 Ma.

5.4.3 Ar-Ar data of tuff samples from the Emborozú Formation

Abapó-1

The sample Abapó-1 has a total gas age of 2.05 ± 0.22 Ma. Relatively old dates (~4.5 Ma for the first step) exist in the low-temperature steps and a fairly flat age spectra exists during the later temperature steps. These steps result in a plateau age of 1.96 ± 0.06 Ma for steps 4 to 7 (Fig. 5.8B). The K/Ca-ratio shows very slightly decrease for the region of the plateau age (Fig. 5.8B). The $^{40}Ar/^{36}Ar$-intercept of steps 4 to 7 is with 286 ± 84 equal to the atmospheric intercept, resulting in an isochron age of 2.00 ± 4.20 Ma (Fig. 5.8B). However, the high K/Ca-ratios of the first steps suggest that all steps have to be included in the age interpretation. Therefore, we assume that the total gas age of 2.05 ± 0.22 Ma is the most probably age of the Abapó-1 sample.

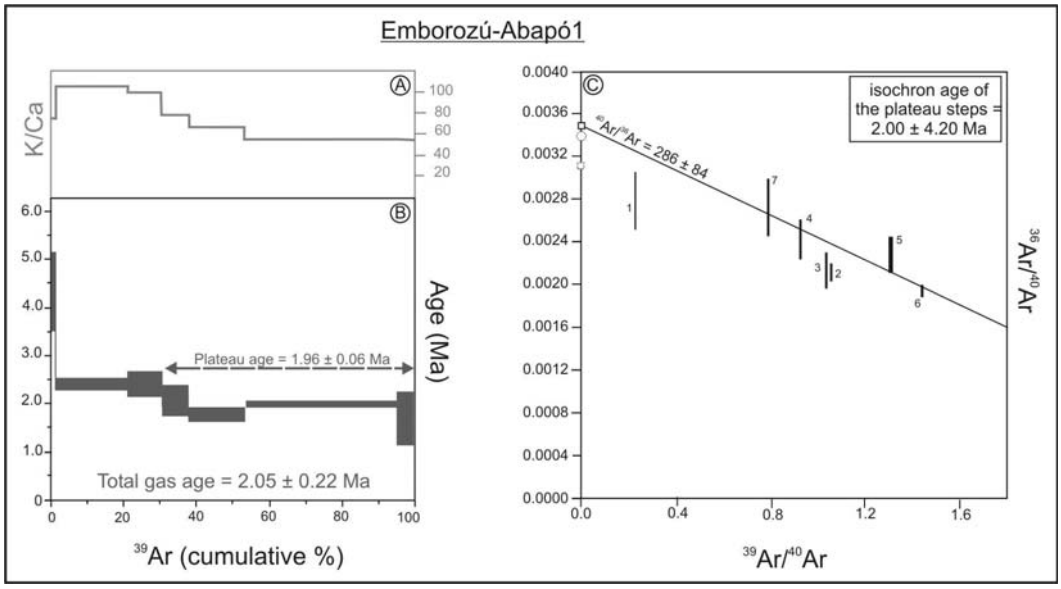

Fig. 5.8: Radiometric data of biotite sample Abapó-1. (A) Plot of the K/Ca-ratio versus cumulative ^{39}Ar; (B) $^{40}Ar/^{39}Ar$ incremental heating age spectra; (C) $^{40}Ar/^{39}Ar$ inverse isochron diagram. Circle shows the atmospheric $^{40}Ar/^{36}Ar$-ratio, grey dashed line is the intercept of all data points, and black solid line represents the intercept of the integrated age. See text for discussion. The result of each step is given in Appendix E. Analytical uncertainties are reported at the 2σ level.

EMB-01

Sample EMB-01 (total gas age = 7.8 ± 1.1 Ma) exhibits very young dates in the low-temperatures steps (1.79 ± 0.41 Ma) and roughly flat steps in the intermediate- and high-temperature range (between 6.0 and 8.5 Ma, see Fig. 5.9B). The steps 3, 5, and 6 show an integrated age of 8.07 ± 0.41 Ma and an intercept age of 8.32 ± 0.36 Ma (Fig. 5.9C). The isochron age of steps 3, 5, 6 yield 8.43 ± 0.32 Ma . However, the K/Ca-plot (Fig. 5.9A)

excludes all steps for biotite age interpretation except step 3 because of their low to very low K/Ca-ratios. Therefore, sample EMB-01 will not be included in the discussion below.

EMB-02

The sample EMB-02 has a total gas age of 7.50 ± 2.30 Ma (Fig. 5.9B). Because of the very low potassium content, this age is unreliable (Fig. 5.9A). The sample EMB-02 will not be mentioned in the following discussion because of the very low to zero K/Ca-ration.

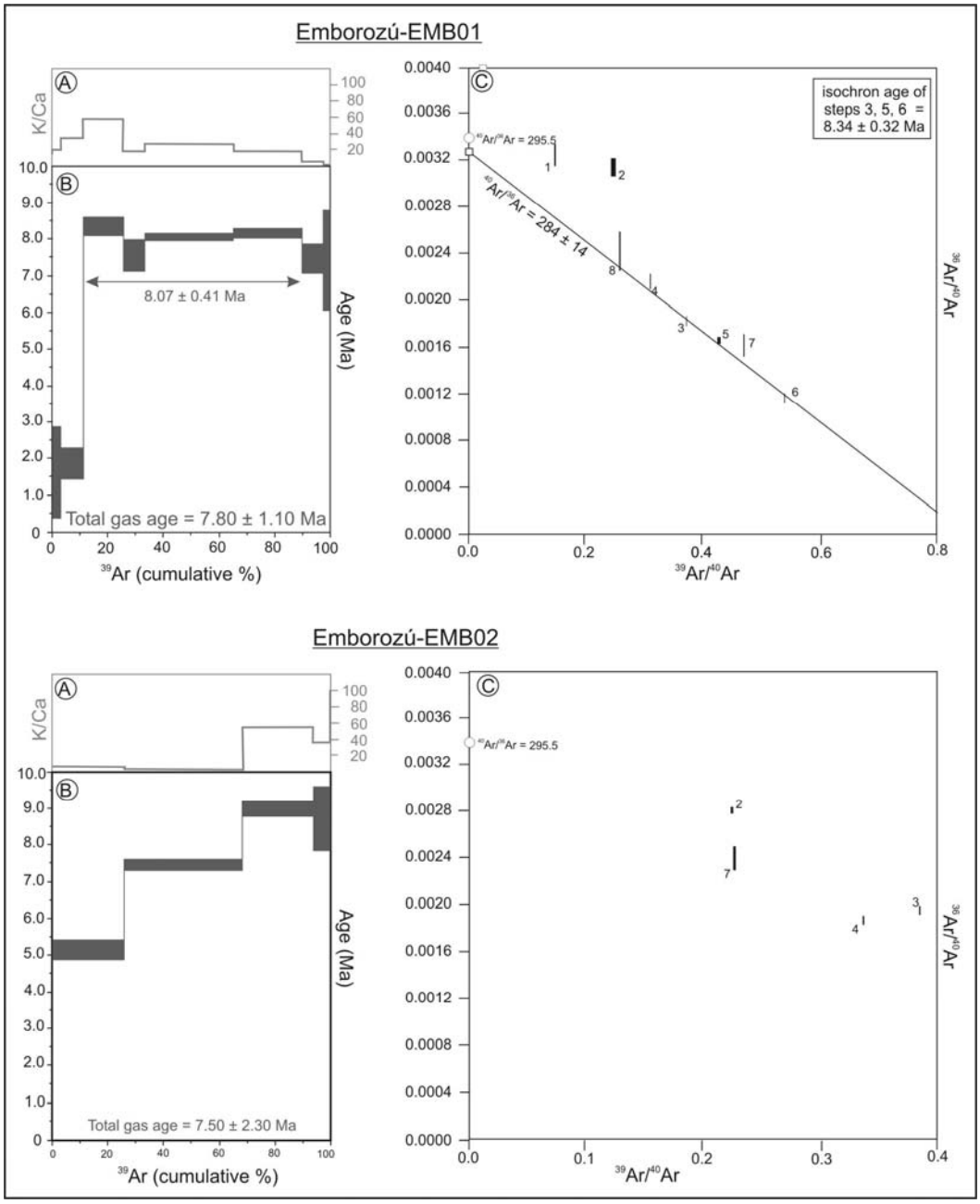

Fig. 5.9: Radiometric data of biotite samples EMB-01 and EMB-02. (A) Plot of the K/Ca-ratio versus cumulative ^{39}Ar; (B) $^{40}Ar/^{39}Ar$ incremental heating age spectra; (C) $^{40}Ar/^{39}Ar$ inverse isochron diagram. Circle shows the atmospheric $^{40}Ar/^{36}Ar$-ratio, grey dashed line is the intercept of all data points, and black solid line represents the intercept of the integrated age. See text for discussion. The result of each step is given in Appendix E. Analytical uncertainties are reported at the 2σ level.

EMB-04

The total gas age for sample EMB-04 is 7.86 ± 0.28 Ma. The step heating exhibits fairly flat age spectra with discordant dates appearing in step 4, 5, and 7. The integrated age of the flat steps 2 and 3 yields 8.10 ± 0.08 Ma (Fig. 5.10B) and account for an isochron age of 8.20 ± 0.11 Ma (Fig. 5.10C). The K/Ca-ratio is high for the low temperature steps (2-3) and decreases significantly to the higher-temperature steps (Fig. 5.10A). However, the two steps exceed ~32 % cumulative Ar, too low for a reliable interpretation. A likely depositional age of the biotite sample EMB-04 is its total gas age (7.86 ± 0.28 Ma).

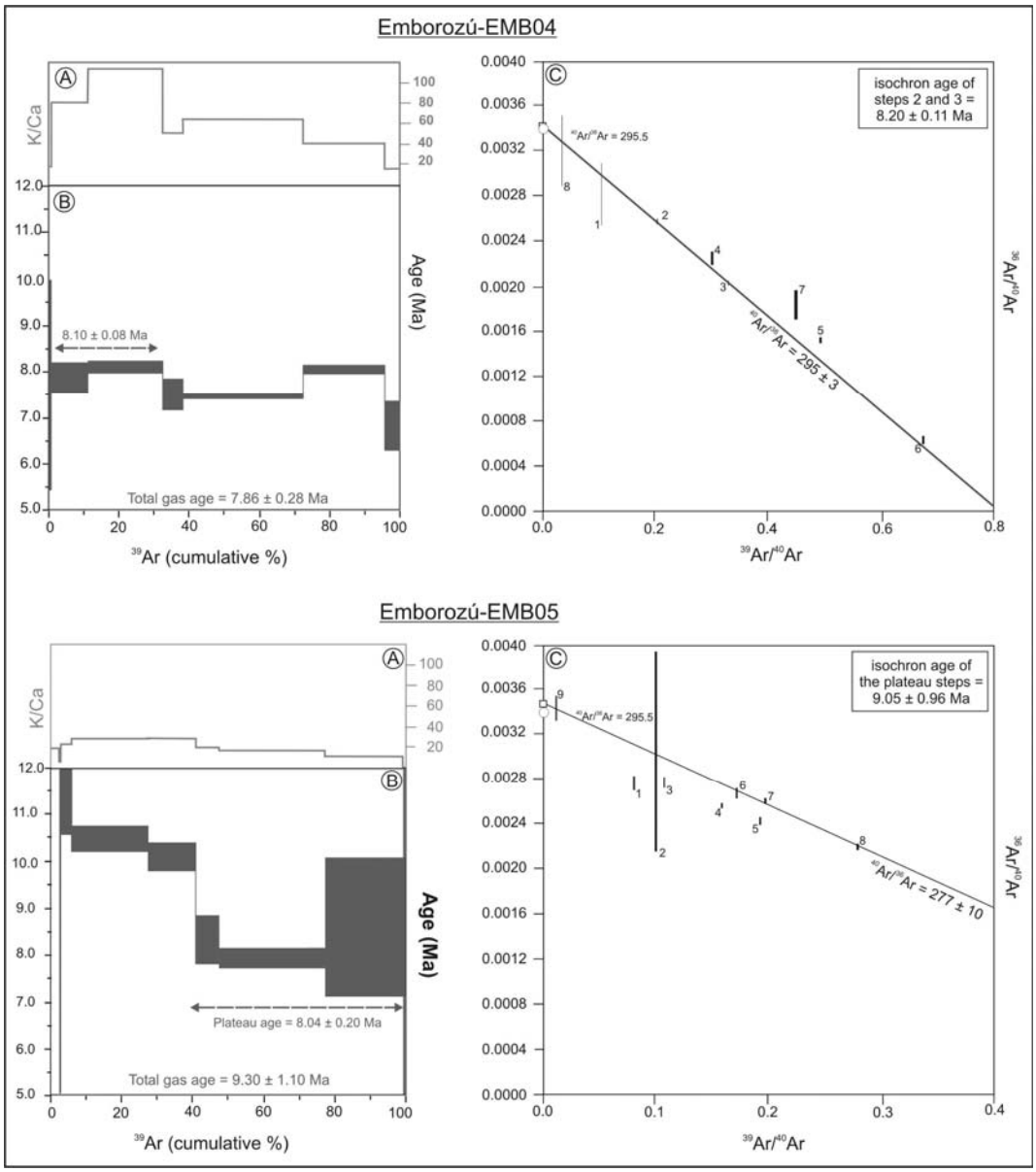

Fig. 5.10: Radiometric data of biotite samples EMB-04 and EMB-05. (A) Plot of the K/Ca-ratio versus cumulative ^{39}Ar; (B) $^{40}Ar/^{39}Ar$ incremental heating age spectra; (C) $^{40}Ar/^{39}Ar$ inverse isochron diagram. Circle shows the atmospheric $^{40}Ar/^{36}Ar$-ratio, grey dashed line is the intercept of all data points, and black solid line represents the intercept of the integrated age. See text for discussion. The result of each step is given in Appendix E. Analytical uncertainties are reported at the 2σ level.

EMB-05

The total gas age for sample EMB-05 is 9.30 ± 1.10 Ma. The incremental heating plot shows a low-temperature "staircase" and a plateau at high-temperatures (Fig. 5.10B). This flat describes a plateau age of 8.04 ± 0.20 Ma (steps 6-9); the intercept of the plateau steps is slightly lower than the atmospheric intercept with 277 ± 10 and yields an isochron age of 9.05 ± 0.96 Ma (Fig. 5.10C). However, the K/Ca-ratios (Fig. 5.10A) are too low for a biotite sample; therefore, we will eliminate sample EMB-05 from the discussion below.

5.4.4 Ar-Ar data of tuff sample CH-095

Sample CH-095 represents a total gas age of 0.32 ± 0.09 Ma. The initial step displays decreasing old dates and the later stage present a flat region. This flat yields a plateau age of 0.29 ± 0.09 Ma for the steps 3-9 (Fig. 5.11B). The intercept of these data points is with 288 ± 13 equivalent to the atmospheric ratio and represents an age of 0.38 ± 0.19 Ma (Fig. 5.11C). The K/Ca-plot in Fig. 5.11A shows decreasing K/Ca-ratios for the plateau steps from left to right. However, the plateau age represent the best depositional age of sample CH-095 with 0.29 ± 0.09 Ma.

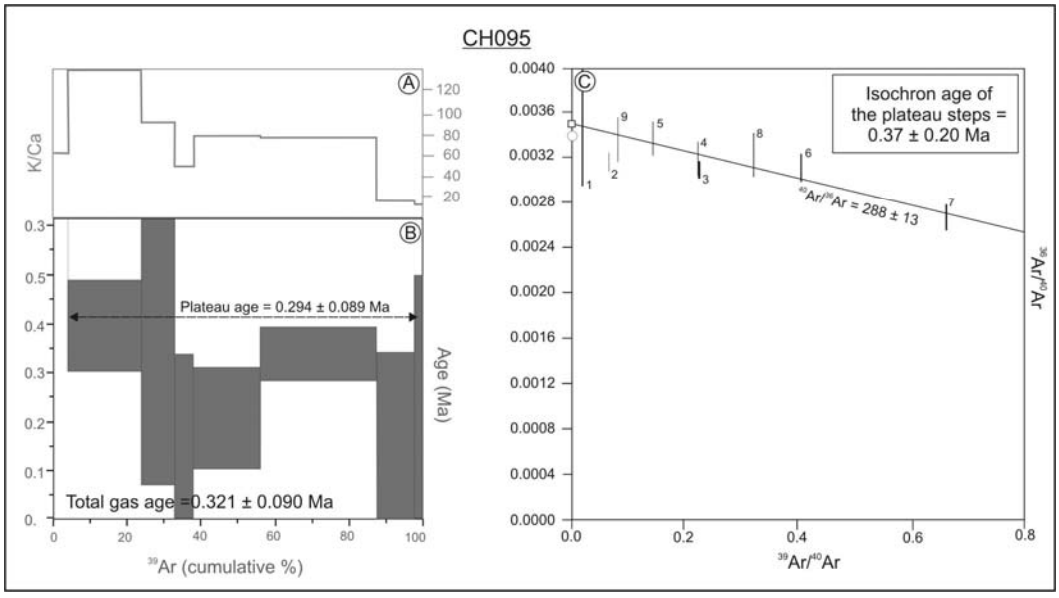

Fig. 5.11: Radiometric data of biotite samples CH-095. (A) Plot of the K/Ca-ratio versus cumulative ^{39}Ar; (B) $^{40}Ar/^{39}Ar$ incremental heating age spectra; (C) $^{40}Ar/^{39}Ar$ inverse isochron diagram. Circle shows the atmospheric $^{40}Ar/^{36}Ar$-ratio, grey dashed line is the intercept of all data points, and black solid line represents the intercept of the integrated age. See text for discussion. The result of each step is given in Appendix E. Analytical uncertainties are reported at the 2σ level.

5.5 Summary of results

In the following paragraph, I summarize radiometric ages of each sample and relate the results to the stratigraphic development (Tab.5.2).

Tab. 5.2: Radiometric dates of each measured sample compared with the lithologies and the formation Abbreviations: b = boulder, sst = sandstone, ms = mudstone, mg = medium-grained, fg = fine-grained.

Sample	Age (Ma) ± 2σ	Lithology	Formation
CH-095	0.3 ± 0.1	unconsolidated sandy material	Pleistocene
Abapó-1	2.1 ± 0.2	well rounded clast of b size and mg, yellow sst	Emborozú
EMB-04	7.9 ± 0.3	muddy, dark red to grey sst and b	Emborozú
EMB-06	9.1 ± 0.7	ms-rich overbank with fg sst	Tariquia
EMB-07	10.5 ± 0.3	ms-rich overbank with yellow fg-mg sst	Tariquia
EMB-10	9.7 ± 0.6	channeled fg yellow sst and red ms	Tariquia
EMB-11	8.8 ± 0.7	channeled fg yellow sst and red ms	Tariquia
CH-01	9.4 ± 0.5	red mg sst and red to brown ms	Tariquia
CH-318	23.5 ± 5.2	massive mg yellow sst and subordinate brown ms	Petaca

Petaca Formation

The only radiometric age data of the Petaca Formation, sample CH-318 from Itapú section, shows a staircase profile with no plateau age. The total gas age is 23.5 ± 5.2 Ma (Tab. 5.2), whereas the youngest date indicates a depositional age ≤ 18.6.

Tariquia Formation

We measured radiometric ages from six biotite samples from three sections in the Subandean-Chaco basin. However, our only data point from the western Chaco Basin, sample CH-160 from Masavi section, is valid because of very low K/Ca-ratios. Sample CH-01 from section Chiquiaca has no plateau age but shows a useful K/Ca-ratio with a total gas age of 9.4 ± 0.5 (Tab. 5.2). Samples EMB-06, EMB-07, EMB-10, and EMB-11 from section Emborozú do not represent plateau ages and display high to low K/Ca-ratios. The total gas ages of these biotite samples range between 9.1 ± 0.7 Ma and 10.5 ± 0.3 Ma (Tab. 5.2).

Emborozú Formation

We measured radiometric ages from five biotite samples from two sections in the Subandean-Chaco Basin. Sample Abapó-1 suggests a depositional age of the upper Emborozú of 2.0 ± 0.4 Ma. Biotite samples EMB-01, EMB-02, EMB-04, and EMB-05 are deposited within section Emborozú. However, the K/Ca-ratios of the samples EMB-01, EMB-02, and EMB-05 are too low to warrant further consideration. The radiometric age of sample EMB-04 suggest a depositional age of 7.9 ± 0.3 Ma (Tab. 5.2).

Sample CH-095

The radiometric age of sample CH-095 from the unconsolidated, horizontal strata is 0.3 ± 0.1 Ma (Tab. 5.2).

5.6 Discussion of the Cenozoic basin fill development

Echavarria et al. (2003), Jordan et al. (1997) and several other authors suggested that the Cenozoic foreland basin stratigraphy developed diachronously, whereby the age of the foreland basin depozones and their sedimentary units (formations) should decrease from west to east, along with the eastward progradation of the deformation front (e.g. Gubbels et al., 1993; Dunn et al., 1995; Moretti et al., 1996; Kley et al., 1997; DeCelles and Horton, 2003; Ege, 2004). Jordan et al. (1997) also described southwardly decreasing depositional ages of the stratigraphic units, parallel to the structural trend.

Our new age data extend along two east-west striking profiles. The northern profile between 17°-20° S (Fig. 5.12) is based on new data as well as data from Marshall and Sempere (1991), Marshall et al. (1993), Moretti et al. (1996), Jordan et al. (1997), and McQuarrie et al. (2005). The southern profile between 21°-23° S (Fig. 5.14) comprises new data as well as data from Marshall and Sempere (1991) and Echavarria et al. (2003).

Northern profile

No age data exist for the Petaca Formation in the western Subandean. A tuff has been dated by Erikson and Kelley (1995) and Jordan et al. (1997) approximately 400 m above the Tariquia base in Monteagudo (Fig. 5.1 and 5.12). The tuff is interbedded within sandstones and shales of a floodplain environment and indicates a depositional age of 24.4 ± 2.6 Ma, implying that foreland basin development in the present-day western Subandean started >25 Ma (Erikson and Kelley, 1995; Jordan et al., 1997) with the deposition of the Petaca Formation. The depositional age of the Petaca-base is given as ~27 Ma by Marshall and Sempere (1991), based on mammal bones along the Quebrada Saguayo in the westernmost Chaco (Fig. 5.12).

No age data exist for the Petaca-Yecua contact in the western Subandean. However, the depositional age of the Yecua Fm started >25 Ma, based on a single tuff bed (Erikson and Kelley, 1995; Jordan et al., 1997). The age of sample CH-318 (Fig. 5.1 and 5.12) representing medium- to coarse-grained, red sandstones of the Petaca Formation, suggests a minimum age (approximately 15 m under the Petaca-Yecua boundary) of ≤18.6 Ma for the top of the Petaca Formation (Fig. 5.12). Shallow-marine foraminifera, of the Yecua Formation in the northwestern Chaco (e.g. Abapó and Angostura sections), suggest that the Petaca-Yecua boundary is ≥14 Ma old in the northwestern Chaco (Fig. 5.1 and 5.12).

The age of the Yecua-Tariquia boundary is constrained by a radiometric age date from the basal Tariquia-base in Monteagudo (mentioned above) as <24.4 Ma (Erikson and Kelley, 1995; Jordan et al., 1997). However, in the northwestern Chaco (Abapó and Angostura; see Fig. 5.1 and 5.12) shallow marine foraminifera of the Yecua Formation suggest a much younger, late Miocene (≥7 Ma, chapter 3) age (Fig. 5.12).

No radiometric age data exist for the age of the Tariquia-Guandacay contact in the northern transect; likewise there are no age data for the Emborozú-Guandacay contact. However, DeCelles and Horton (2003) described that the deformation front reached the western Subandean at 20° S in the late Miocene, probably after 10 Ma (Gubbels et al., 1993). Because the facies of the Emborozú Formation implies a very proximal position to the deformation front we suggest a basal Emborozú age in the western Subandean of ≤10 Ma (as did McQuarrie et al., 2005). In the northwestern Chaco (Abapó, see Fig. 5.12) Moretti et al.

(1996) gave an age of 3.3 Ma at the Guandacay-Emborozú boundary. Our age (Abapó-1) from the upper Emborozú Formation in the same section reports an age of 2.0 ± 0.1 Ma.

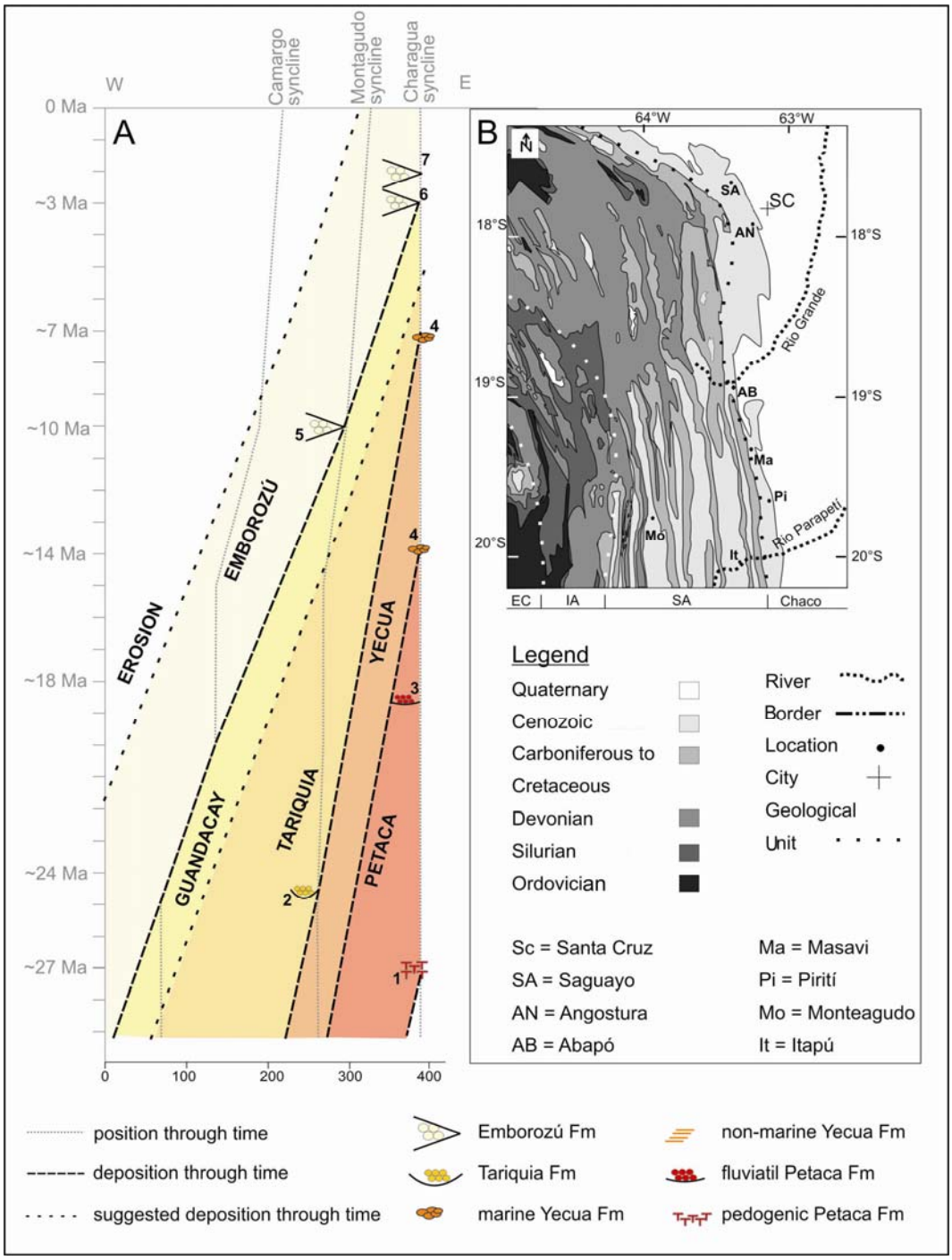

Fig. 5.12: (A) Basin migration diagram for the Central Andean backarc region between 18° S and 20° S. (B) Simplified geological map of the northern Subandean-Chaco basin between 17° S and 20° S (modified from Pareja et al., 1978). Abbreviations: EC = Eastern Cordillera, IA = Interandean, and SA = Subandean. Numbers refer to sources as follows: 1 = biostratigraphic correlation from Marshall and Sempere (1991). 2 = age from Jordan et al. (1995). 3 = age of sample CH-318. 4 = biostratigraphic correlation of marine foraminifera (chapter 3). 5 = fold-thrust movement (Gubbles et al., 1993, McQuarrie et al., 2005). 6 = age from Moretti et al. (1996). 7 = age of sample Abapó-1.

Southern profile: between 21° S - 23°S

Age data are rare for the lowermost Petaca and Yecua Formation in the southern part of the Subandean-Chaco foreland basin are. However, Echavarria et al. (2003) published magnetic-polarity stratigraphy data from Subandean sediments deposited in northernmost Argentina. Fig. 5.13, compares the stratigraphy of northwestern Argentina with the Cenozoic Chaco deposits.

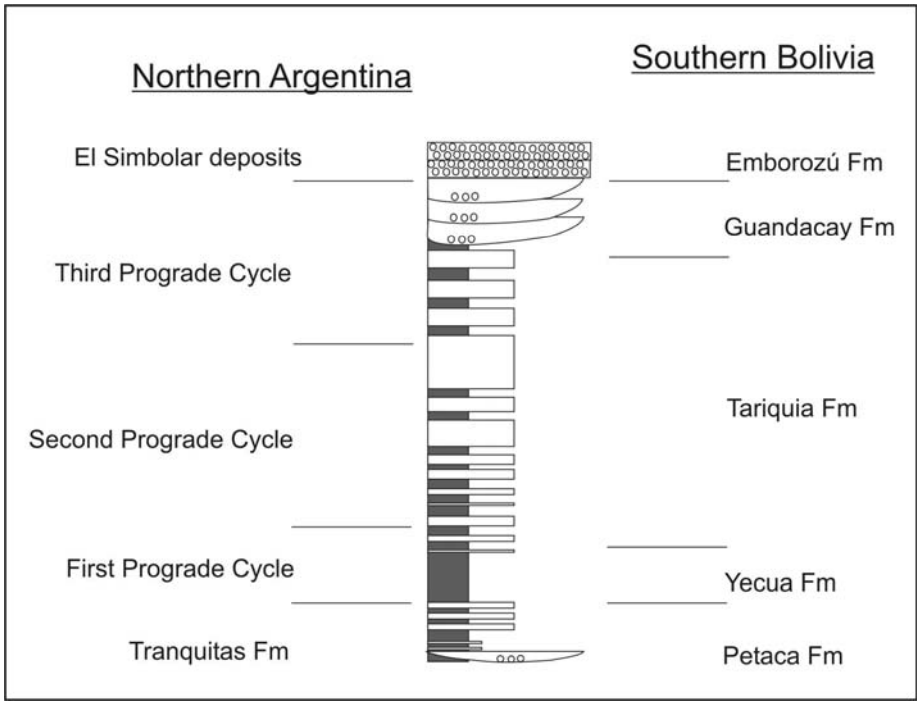

Fig. 5.13: Comparison of stratigraphic units from northern Argentina and southern Bolivia (after Echavarria et al., 2003; and own data).

The basal Cenozoic foreland basin deposit in Argentina is known as Tranquitas Formation, equivalent to the Petaca Formation in southern Bolivia. This formation is overlain by three "progradational cycles" (Echavarria et al., 2003), approximately corresponding to the Yecua, Tariquia, and Guandacay Formation equivalents. The uppermost, El Simbolar deposits (Echavarria et al., 2003) are equivalent to the Emborozú Formation.

Echavarria et al. (2003) document an eastwardly younging trend of the Tranquitas Formation and the "first prograde cycle", dated by magnetic-polarity stratigraphy. The top of the Tranquitas Formation is ~13 Ma old in the Simbolar syncline but only ~9.5 Ma old near Bermejo (Fig. 5.14); the top of the "first prograde cycle" youngs from ~12.5 Ma in the Simbolar Syncline to ~8.5 Ma near Bermejo and to >7 Ma within the Seco syncline (Fig. 5.14).

Our new radiometric ages of the Tariquia Formation from the Emborozú section (south-westernmost syncline in the Subandean, Fig. 5.1 and 5.14) range between 9.1 ± 0.7 Ma and 10.5 ± 0.3 Ma. Further east, in the Simbolar Syncline, the equivalent Argentinean unit ranges between 12.5-4.0 Ma, 8.5-5 Ma in Bermejo, and 7-2.5 Ma in the westernmost syncline of the Subandean (Seco syncline; Fig. 5.14, Echavarria et al., 2003).

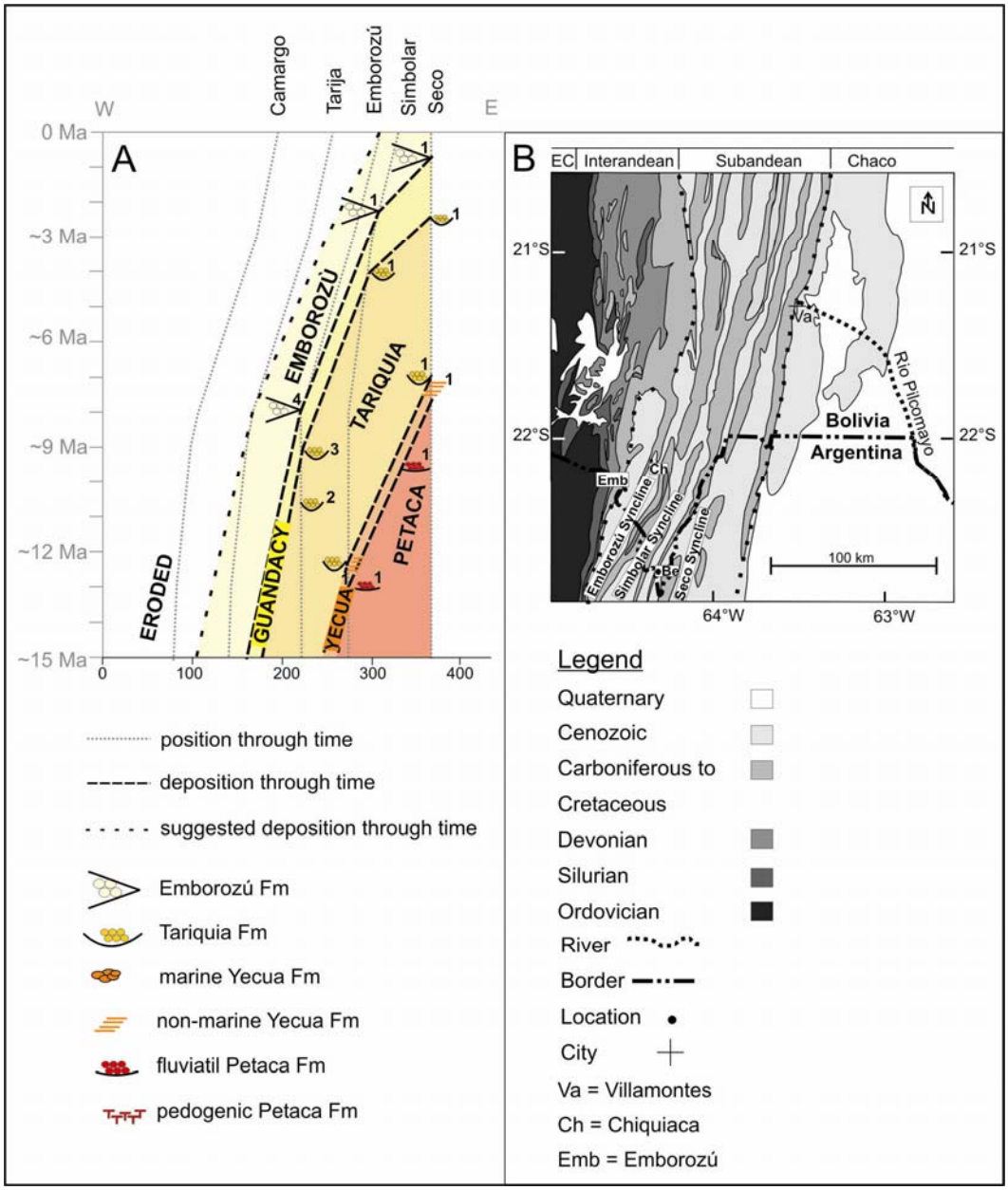

Fig. 5.14: (A) Basin migration diagram for the southern transect between 21° and 23°S (B) Simplified geological map of the northern Subandean-Chaco basin between 20.5° and 23°S modified from Pareja et al. (1978) with the following abbreviations: EC = Eastern Cordillera. Numbers refer to sources as follows: 1 = magnetic-polarity stratigraphy from Echavarria et al. (2003). 2 = age of sample EMB-06. 3 = age of sample EMB-11. 4 = age of samples EMB-01, EMB-04, EMB-05.

The new radiometric ages constrain the age of the Guandacay Formation in the Emborozú syncline as 9-8 Ma old. However, Guandacay-equivalent strata within the Simbolar syncline document a depositional age between 4.0-2.2 Ma (Echavarria et al., 2003). Echavarria et al. (2003) suggested that the depositional age of the Guandacay-equivalent strata range between 5.0-2.5 Ma in Bermejo, whereas Marshall and Sempere (1991) denote a depositional age of Huayquerian time (12.0-5.3 Ma), indicated by the occurrence of a notoungulate at the base of the Guandacay Formation. The easternmost dataset (Seco syncline) of Echavarria et al. (2003) reports a depositional age between 2.5-2.2 Ma for Guandacay-equivalent strata.

The basal Emborozú Formation is dated by sample EMB-04 as old as 7.9 ± 0.3 Ma along the Emborozú syncline, the westernmost Subandean synclines in this region. However,

Echavarria et al. (2003) dated the stratigraphically equivalent Emborozú Formation as 2.2 Ma within the Simbolar syncline (western Subandean) and <1 Ma in the Seco syncline (eastern Subandean).

The chronological development of the Guandacay Formation (proximal foredeep tectofacies) and the Emborozú Formation (wedge-top tectofacies) is not uniformly decreasing from west to east. Although the Emborozú Formation was deposited in the westernmost syncline of the Subandean ≤8 Ma, the eastward synclines indicate wedge-top development only since ≤2.2 Ma. And although the Guandacay Formation was deposited in the westernmost syncline of the Subandean since 4 Ma, eastward synclines indicate proximal foredeep development as 0.8 Ma. This "time gap" of 3-4 Ma is founded in the structural development of the Interandean and the western Subandean, as well as in their locations with respect to the Interandean to the west. Echavarria et al. (2003) described an early phase of shortening (between 9-8.5 Ma), which built the Cinco Picachos anticline back-thrust (west of the Emborozú syncline) and a proto-Pescado uplift (west of the Simbolar syncline). However, the proto-Pescado uplift was lower than the sedimentation rate. The Cinco Picachos structure generated a proximal foredeep to wedge-top position for the Emborozú syncline, documented by 9-8 Ma old Guandacay Formation and 8 Ma old Emborozú Formation while in the eastern synclines high sedimentation rates of Tariquia–equivalent strata suggest a central foredeep depozone (Echavarria et al., 2003). The uplift of the Subandean anticlines of east Cinco Picachos anticline did not exceed the sedimentation rate until the early Pliocene. The Pescado uplift exceeded the sedimentation rate >2 Ma, documented by 2.2 Ma old Emborozú-equivalent deposits.

5.7 Conclusions

Our new radiometric age data document a strongly diachronous development of the Chaco foreland basin. Depositional ages of largely lithologically defined formations decrease primarily to the east, as expected for foreland basin deposits that are situated adjacent to an eastward prograding fold-thrust front, but also along structural strike, i.e. to the south.

The lithostratigraphy, petrography, facies, and radiometric ages suggest that the age of each formation depends on its distance to the deformation front. While the Emborozú Formation represents a coarse-grained facies adjacent to the deformation front (wedge-top depozone), deposits identified as Petaca Formation typically occupy a distal position toward the deformation front (forebulge depozone). This implies that the eastward propagation of the fold-thrust front directly reflects the depositional age of each formation at a certain place. The propagation of the deformation front in space and time during shortening consequently led to a strongly diachronous deposition of the foreland basin formations.

Diachronous propagation of the fold-thrust front and concomitant diachronous foreland basin development occurred also along structural strike. Interandean shortening, for example, started along 20° S at >20 Ma (McQuarrie, 2002), whereas Interandean shortening developed along 21° S between ~10 and 5 Ma (Kley, 1996). Shortening within the Subandean developed in the north since the middle Miocene (<15 Ma, after Lamb and Hoke, 1997) but in the south only since the late Miocene (<9 Ma, after Ege, 2004).

Shortening processes within the Central Andean backarc led to the following foreland basin development:

In the early Miocene (≥18 Ma) foredeep deposits (Tariquia Formation) developed in the northwestern Subandean-Chaco basin, forebulge deposits (Petaca Formation) along the northeastern Subandean-Chaco and in the southern Subandean-Chaco (Fig. 5.15).

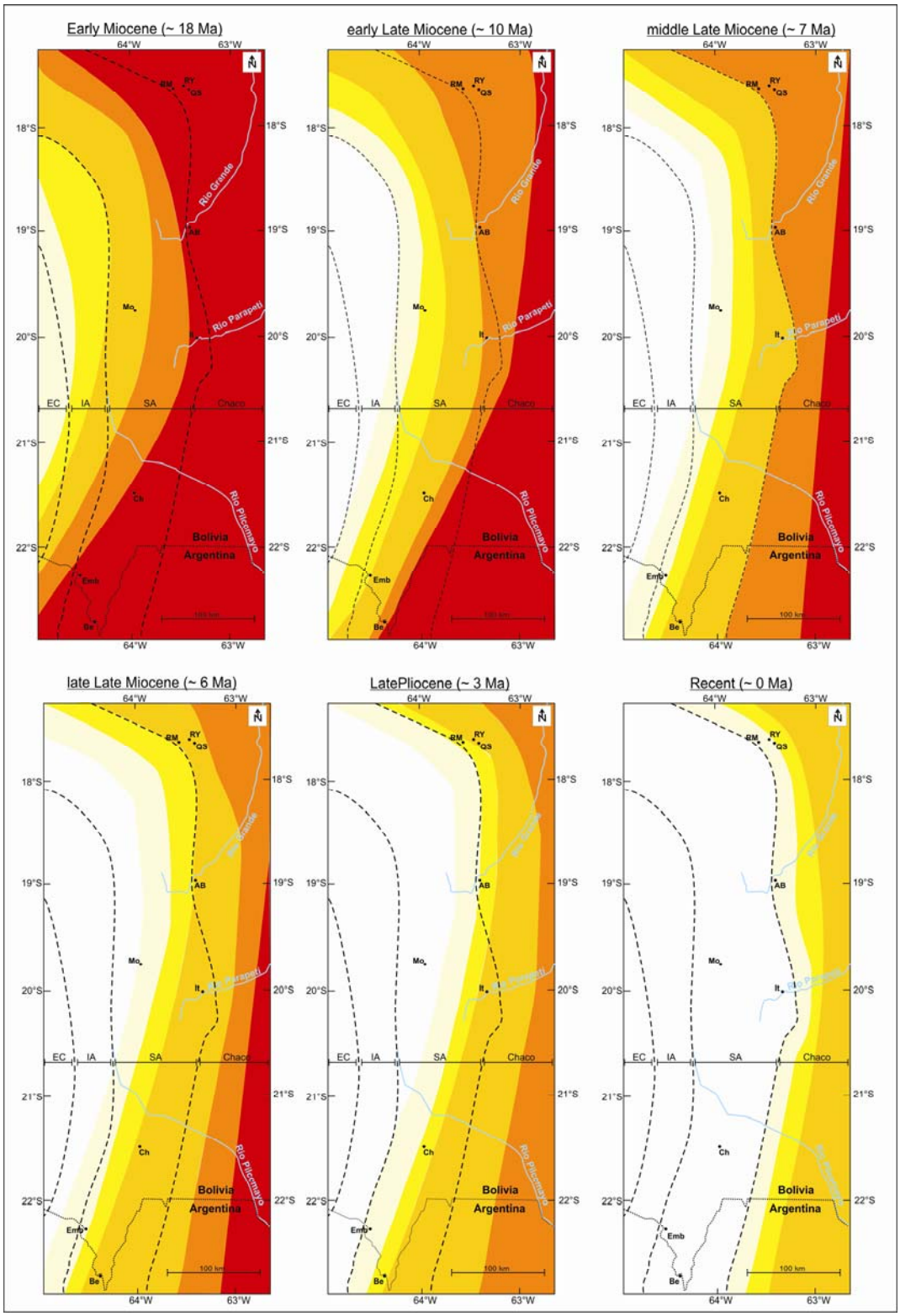

Fig. 5.15: Facies maps throughout the Subandean-Chaco basin for different periods during foreland basin development. Abbreviations as in Fig. 5.13 and 5.14. Colors refer to the following formations: red = Petaca, orange = Yecua, orange-yellow = Tariquia, yellow = Guandacay, light yellow = Emborozú.

In the early late Miocene (~10 Ma) the northwestern part of the Subandean-Chaco basin accumulated wedge-top deposits (Emborozú Fm), in the northeastern part developed a very distal foredeep depozone through the marine Yecua Formation, the southwestern part indicated a foredeep development (Tariquia and Tariquia-equivalent formation), and in the southeast deposits indicate a forebulge depozone (Petaca-equivalent, see Fig. 5.15) appear.

In the middle late Miocene (7-6 Ma), the deformation propagated through the northwestern Subandean-Chaco basin and a wedge-top depozone developed along the northwestern Subandean (Emborozú Formation). In the northeast, a distal (~7 Ma, Tariquia Formation) to proximal (<6 Ma, Guandacay Formation) foredeep basin developed. In the southern Subandean-Chaco basin, the propagation of the foreland basin depozones paused (Fig. 5.15).

In the late Pliocene (~3 Ma) the northwestern Subandean-Chaco basin represented a zone of fold and thrust belts west of the deformation front, whereas the eastern Subandean was occupied by the deformation front. The present-day Subandean-Chaco border held at that time a wedge-top position (Emborozú Formation). In the southern Subandean-Chaco basin, the eastward propagation of the foreland basin depozones resumed and led to the development of wedge-top conditions (Emborozú Formation) throughout the southwestern Subandean-Chaco basin. In the southeastern Subandean-Chaco basin, Tariquia-equivalent strata, reflecting central foredeep depozone (Fig. 5.15), were deposited.

The present-day situation is not well determined because the Chaco Basin is mainly covered by Quaternary deposits. However, between the Subandean-Chaco border and the deformation front, we suggest the existence of a wedge-top depozone. Our seismic study (Appendix G) shows blind thrusts in the subsurface which are typical for a wedge-top depozone. East of the deformation front, we suggest the development of an eastward-fining foredeep depozone (Fig. 5.15).

Acknowledgments

This research project represents part of the senior author's Ph.D. thesis and is supported by the SFB 267 and Chaco S.A., Santa Cruz, Bolivia. We thank Prof. José Viramontes (Salta/Argentina) and his group who made his laboratory available and gave a helping hand in processing the samples. Markus Raitzsch did much of the sample preparation. We also thank Konrad Hammerschmidt and the Research Group of Prof. Igor Villa (Bern/Switzerland) for intensive help during the analyses and Jörg Giese for his backup during the analysis.